J Mater Sci (2011) 46:3646–3652
DOI 10.1007/s10853-011-5281-6

Constitutive descriptions for hot compressed low-pressure rotor steel at elevated high temperature

Xiao-Ling Fang · Ding-Jian Jiang

Received: 14 December 2010 / Accepted: 12 January 2011 / Published online: 4 February 2011

Abstract The constitutive equation of the material is an essential ingredient of any structural calculation. In this article, a phenomenological constitutive model is established to describe the dynamic deformation behavior of 30Cr2Ni4MoV steel in wide strain rate, strain, and temperature ranges. Also, the mathematical models to predict peak stress and corresponding strain were obtained. The stress–strain values predicted by the developed model well agree with experimental results, which confirmed that the developed constitutive equation gives an accurate and precise estimate for the flow stress of 30Cr2Ni4MoV steel.

Introduction

A reliable constitutive model is necessary to describe properly the dynamic response of a material under a deformation with wide range of forming temperature, strain rate, and strain. Meanwhile, numerical simulations can be truly reliable only when a proper material flow stress relationship is built because of its effective role on metal flow pattern as well as the kinetics of metallurgical transformation. Therefore, a number of constitutive models have been proposed to describe the strain rate and temperature-dependent behavior of materials [1–12]. Lin and Liu [2] developed a comprehensive constitutive model, in which one innovative material parameter L was proposed, to predict stress–strain curve up to the peak stress for 42CrMo steel. Spathis [3] anticipated the contribution of the main features of plastic behavior, such as yielding, rate effect, isotropic, and kinematic hardening, through a new approximation of the constitutive equation with a visco-plastic term, as well as a new consideration of the functional form of the rate of plastic deformation. Considering the effects of the strain and strain rate, some modified models were developed to describe the relationships of the flow stress, strain rate, and temperature of 42CrMo steel and 2124-T851 aluminum alloy over a wide range of temperature and strain rate [5, 6]. Lin et al. [7] divided the whole thermal deformation process of most metal material into four stages. Stage I (work hardening stage), stage II (transition stage), stage III (softening stage), and stage IV (steady stage). Based on the classical stress–dislocation relation and the kinematics of the dynamic recrystallization, they established the flow stress constitutive equations of the work hardening-dynamical recovery period and dynamical recrystallization period for 42CrMo steel, respectively. Considering the coupling effects of strain rate-temperature-strain, a combined Johnson-Cook and Zerilli–Armstrong (JC–ZA) model, and a modified JC model were developed to describe the relationship of the flow stress, strain rate, and forming temperature for a typical high-strength alloy [8, 9]. Also, some other researchers [13–15] developed some effective artificial neural network (ANN) models to predict the hot deformation behavior of the alloy or metals and their results show that the ANN model can accurately predict hot deformation behavior of alloys or metals.

The prediction of flow stress for 30Cr2Ni4MoV steel is very important for the practical industrial production of the large rotor. In this study, a phenomenological constitutive model, which is based on the attenuation coefficient (L) proposed by Lin and Liu [2], has been established to describe dynamic deformation behavior of 30Cr2Ni4MoV steel in wide strain rate, strain, and temperature ranges. The

X.-L. Fang (✉) · D.-J. Jiang
Department of Chemical and Petroleum Engineering, Karamay Vocational and Technical College, Xinjiang 833600, China
e-mail: xjfangxl@163.com

validity of predicted stress–strain curves from the developed constitutive models is discussed.

Experiments and results

30Cr2Ni4MoV steel is widely used in the nuclear power generation. The chemical composition of 30Cr2Ni4MoV is (wt%): 0.28C-1.85Cr-3.35Ni-0.42Mo-0.089V-0.22Mn-0.06Si-0.004P-0.002S-0.007Al-0.06Cu-0.004Sn-0.0044As-0.0009Sb. Cylindrical specimens with a diameter of 10 mm and a height of 12 mm were used. In order to minimize the frictions between the specimen and fixtures during hot deformation, the flat ends of the specimen were recessed to a depth of 0.1 mm deep to entrap the lubricant of graphite mixed with machine oil. According to the practical industrial production of the large 30Cr2Ni4MoV steel rotor, the processing parameters are well selected. The hot compression tests were performed on Gleeble-1500 thermo-simulation machine in the four different temperatures (1223, 1323, 1423, and 1523 K) and three different strain rates (0.001, 0.01, and 0.1 s^{-1}). The specimens were heated to 1573 K at a heating rate of 10 K s^{-1} by thermo-coupled feedback-controlled AC current, and held for 5 min. Then, the specimens were cooled at 10 K s^{-1} to the forming temperature and held for 3 min at isothermal conditions before compression tests, to obtain the heat balance. Some more detailed experimental procedures can be found in reference [16].

Constitutive equations of flow stress for 30Cr2Ni4MoV steel

From the measured stress–strain data, the work hardening rate ($\theta = d\sigma/d\varepsilon$) can be calculated, and the work hardening rate-stress curves show that the work-hardening rate decreased continuously with the increase of the stress, and an inflexion point close to the peak stress appears in the austenite domain [17, 18]. Lin and Liu [2] formulated the work hardening rate, θ, as the following linear function of flow stress.

$$\theta = \frac{\partial\sigma}{\partial\varepsilon} = L\sigma + B, \tag{1}$$

where L is one material parameter, B is a material constant. When the peak stress appears, the value of θ is equal to zero. So, the value of B can be easily evaluated as $-L\sigma_p$ by Eq. 1. Considering the following boundary conditions,

$$\sigma = \sigma_p,\ \varepsilon = \varepsilon_p. \tag{2}$$

The differential Eq. 1 can be transformed to the following expression.

$$\sigma = \sigma_p\left[1 - \left(\frac{\varepsilon_p - \varepsilon}{\varepsilon_p}\right)e^{L\varepsilon}\right], \tag{3}$$

where σ_p is peak stress and ε_p is the strain corresponding to the peak stress. Obviously, the material parameter L actually describes the attenuation degree of the flow stress.

Determination of L parameter

Equation 1 shows L parameter is sensitive to the forming temperature and strain rate. Taking the logarithm of both sides of Eq. 3, gives,

$$\ln\left(\frac{\varepsilon_p}{\sigma_p}\frac{\sigma_p - \sigma}{\varepsilon_p - \varepsilon}\right) = L\varepsilon. \tag{4}$$

From Eq. 4, it can be found that L parameter under studied experimental conditions can be determined using the plots of $\ln\left(\frac{\varepsilon_p}{\sigma_p}\frac{\sigma_p-\sigma}{\varepsilon_p-\varepsilon}\right)$ versus ε, and the values of L parameter are the slopes of the lines, which were used to linearly fit the data points $\left(\ln\left(\frac{\varepsilon_p}{\sigma_p}\frac{\sigma_p-\sigma}{\varepsilon_p-\varepsilon}\right), \varepsilon\right)$. Table 1 gives the values of the measured peak stresses (σ_p) and peak strains (ε_p) under test conditions. Substituting the values of the measured peak stresses (σ_p) and peak strains (ε_p) under test conditions into Eq. 4 can obtain the relationship between$\ln(\frac{\varepsilon_p}{\sigma_p}\frac{\sigma_p-\sigma}{\varepsilon_p-\varepsilon})$and ε. Figure 1 describes the linear plots of $\ln(\frac{\varepsilon_p}{\sigma_p}\frac{\sigma_p-\sigma}{\varepsilon_p-\varepsilon})$ versus ε under the studied forming temperatures and strain rates, and the calculated L parameter under the test conditions can be easily obtained, as shown in Table 2.

For 30Cr2Ni4MoV alloy steel, L parameter is sensitive to the forming temperature and strain rate, and the following expression is assumed.

$$L = a\dot{\varepsilon}^b e^{cT}, \tag{5}$$

where a, b and c are the material constants.

Taking the logarithm of both sides of Eq. 5, gives,

Table 1 Values of the measured peak stress (σ_p, MPa) and peak strain (ε_p) under the studied experimental conditions

$\dot{\varepsilon}(s^{-1})$	σ_p, ε_p	T (°C)			
		950	1050	1150	1250
0.001	σ_p	60.17	39.99	21.79	12.51
	ε_p	0.18	0.14	0.12	0.07
0.01	σ_p	89.23	56.17	38.33	21.92
	ε_p	0.26	0.22	0.18	0.15
0.1	σ_p	128.22	84.99	55.82	40.27
	ε_p	0.36	0.32	0.24	0.24

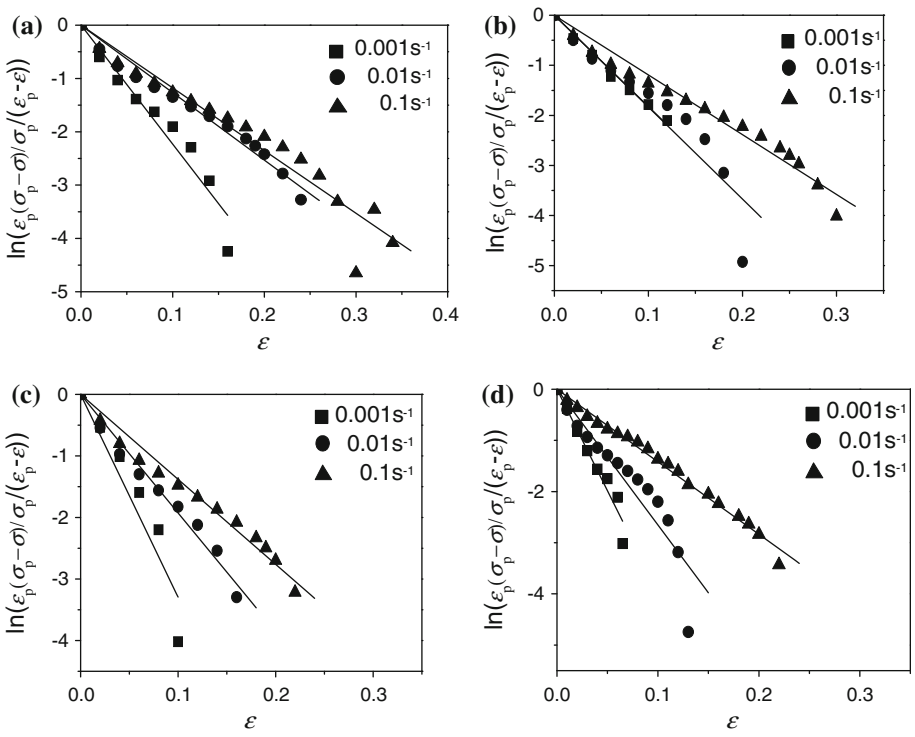

Fig. 1 Linear plot of $\ln(\frac{\varepsilon_p \sigma_p - \sigma}{\sigma_p \varepsilon_p - \varepsilon})$ versus ε for four different strain rates and forming temperatures of **a** 950 °C, **b** 1050 °C, **c** 1150 °C, and **d** 1250 °C

Table 2 Values of L under the studied forming temperatures and strain rates

L (s^{-1})	T (°C)			
	950	1050	1150	1250
0.001	−22.29	−18.25	−32.94	−39.68
0.01	−12.65	−18.35	−19.27	−26.54
0.1	−11.76	−11.92	−13.81	−14.18

$$\ln L = \ln a + b \ln \dot{\varepsilon} + cT. \tag{6}$$

Then, the values of material constants b and c can be obtained from

$$\begin{cases} b = \dfrac{\partial \ln L}{\partial \ln \dot{\varepsilon}} \\ c = \dfrac{\partial \ln L}{\partial T} \end{cases}. \tag{7}$$

The values of material constants b and c can be obtained from the slopes of the lines in the $\ln L - \ln \dot{\varepsilon}$ and $\ln L - T$ plots, respectively, as shown in Fig. 2, and the mean values of b and c can be computed as −0.16 and 0.002, respectively. For the given forming temperature, $\ln a + cT$ is the intercept of $\ln L - \ln \dot{\varepsilon}$ plot. So, material constant a can be evaluated as the averaged value under different forming temperatures. Then, the third material constant a is equal to −0.8. Therefore, the model to calculate L parameter can be expressed as Eq. 8.

$$L = -0.8\dot{\varepsilon}^{-0.16} e^{0.002T}. \tag{8}$$

From Eq. 8 and Fig. 2, it can be easily found that the increase of strain rate will decrease the values of L parameter and increases the flow stress. However, L parameter increases with the increase of the temperatures, meanwhile the flow stress decreases. So, L parameter is an indicator to describe the attenuation degree of the flow stress.

Determination of peak stress σ_p

The Arrhenius equation is widely used to describe the relationship between the strain rate, temperature, and flow stress. It can also be shown as the function of Zener–Hollomon parameter. The hyperbolic law in Arrhenius type equation gives better approximations between Zener–Hollomon parameter and stress [19–24].

$$Z = \dot{\varepsilon} \exp\left(\frac{Q}{RT}\right) \tag{9}$$

$$\dot{\varepsilon} = AF(\sigma) \exp\left(-\frac{Q}{RT}\right), \tag{10}$$

where $F(\sigma) = \begin{cases} \sigma^n & \alpha\sigma < 0.8 \\ \exp(\beta\sigma) & \alpha\sigma > 1.2 \\ [\sinh(\alpha\sigma)]^n & \text{for all } \sigma \end{cases}$ in which, $\dot{\varepsilon}$ is the strain rate (s^{-1}), R is the universal gas constant (8.31 J mol^{-1} K^{-1}), T the absolute temperature (K), Q the activation energy of hot deformation (kJ mol^{-1}), σ the

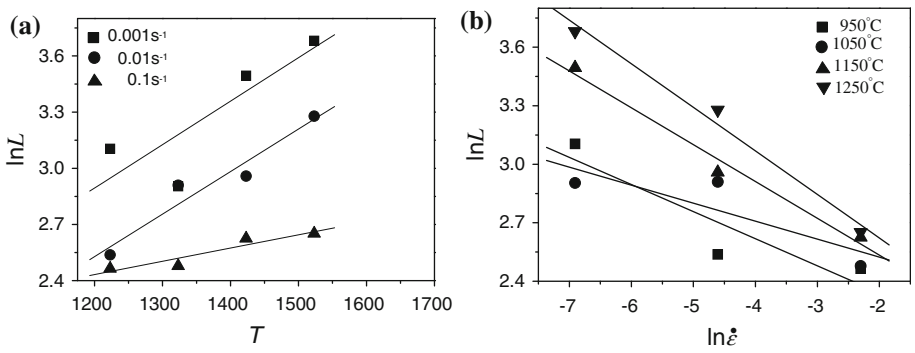

Fig. 2 Linear plots of **a** $\ln L - T$ and **b** $\ln L - \ln \dot{\varepsilon}$.

flow stress (MPa) for a given stain, A, α, and n are the material constants, $\alpha = \beta/n$.

For the low stress level ($\alpha\sigma < 0.8$) and high stress level ($\alpha\sigma > 1.2$), substituting the power law and exponential law of $F(\sigma)$ into Eq. 10, respectively. Then gives,

$$\dot{\varepsilon} = B\sigma^{n'} \tag{11}$$

$$\dot{\varepsilon} = B'\exp(\beta\sigma), \tag{12}$$

where, B and $B'$are the material constants.

Taking the logarithm of both sides of Eqs. 11 and 12, respectively, gives,

$$\ln\sigma = \frac{1}{n'}\ln\dot{\varepsilon} - \frac{1}{n'}\ln B \tag{13}$$

$$\sigma = \frac{1}{\beta}\ln\dot{\varepsilon} - \frac{1}{\beta}\ln B'. \tag{14}$$

Then, substituting the values of peak stress and corresponding strain rate into the logarithm Eqs. 13 and 14 gives the relationship between the flow stress and strain rate, as shown in Fig. 3. The value of $n'$and β can be obtained from the averaged slope of $\ln\sigma - \ln\dot{\varepsilon}$ and $\sigma - \ln\dot{\varepsilon}$plots as 5.2569 and 0.118 MPa^{-1}, respectively. Then, $\alpha = \beta/n = 0.022\,\mathrm{MPa}^{-1}$.

For all the stress level (including low an high stress levels), Eq. 10 can be represented as,

$$\dot{\varepsilon} = A[\sinh(\alpha\sigma)]^n \exp(-Q/RT). \tag{15}$$

Then, the flow stress, σ, can be written as a function of Zener–Hollomon parameter.

$$\sigma = \frac{1}{\alpha}\ln\left\{\left(\frac{Z}{A}\right)^{1/n} + \left[\left(\frac{Z}{A}\right)^{2/n} + 1\right]^{1/2}\right\}. \tag{16}$$

For the given strain rate conditions, differentiating Eq. 15 gives,

$$Q = Rn\frac{d\{\ln[\sinh(\alpha\sigma)]\}}{d(1/T)}. \tag{17}$$

Substituting the values of temperature and peak stress that are obtained from a fixed strain rate into Eq. 17, the value of Q can be derived from the averaged slope of $\ln[\sinh(\alpha\sigma)] - 1/T$ plots (Fig. 4a) as 362.523 kJ mol^{-1}.

Taking the logarithm of both sides of Eq. 15 gives,

$$\ln[\sinh(\alpha\sigma)] = \ln\dot{\varepsilon}/n + Q/(nRT) - \ln A/n. \tag{18}$$

Substituting the values of the strain rate and peak stress for all the tested temperatures into Eq. 18, the relationship between $\ln[\sinh(\alpha\sigma)]$ and $\ln\dot{\varepsilon}$ can be obtained as shown in Fig. 4b. From this figure, it is easy to evaluate the value of material constant A and n as 3.148 $\times$ 10^{11} s^{-1} and 3.544, respectively.

Then, the peak stress constitutive equation of hot deformation for 30Cr2Ni4MoV steel can be expressed as,

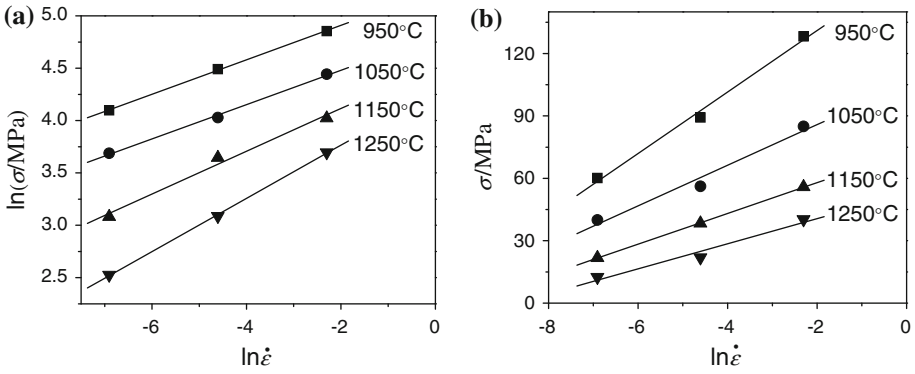

Fig. 3 Relationships between: **a** $\ln\dot{\varepsilon}$ and$\ln\sigma$; **b** $\ln\dot{\varepsilon}$ and σ

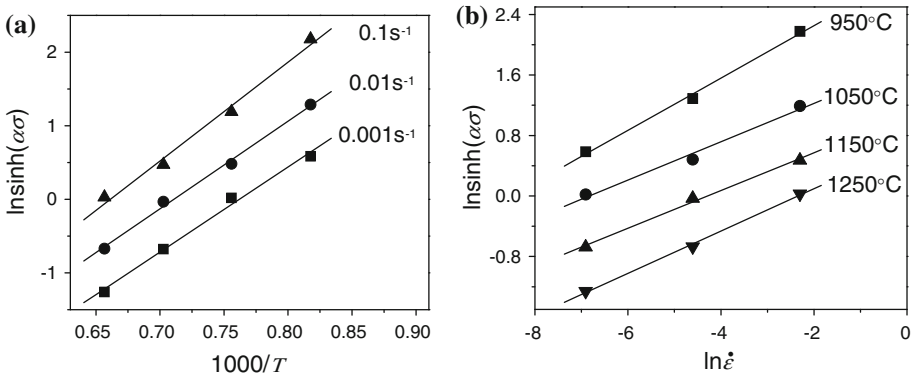

Fig. 4 Relationships between: **a** $\ln[\sinh(\alpha\sigma)]$ and temperature; **b** $\ln\dot{\varepsilon}$ and $\ln[\sinh(\alpha\sigma)]$.

$$\sigma_p = \frac{1}{0.022}\ln\left[\left(\frac{Z}{3.148\times10^{11}}\right)^{1/3.544} + \sqrt{\left(\frac{Z}{3.148\times10^{11}}\right)^{2/3.544}+1}\right]. \quad (19)$$

Also, Zener–Hollomon parameter for 30Cr2Ni4MoV steel can be represented as following,

$$Z = \dot{\varepsilon}\exp[3.625\times10^5/(RT)] = 3.148\times10^{11}[\sinh(0.022\sigma_p)]^{3.544}. \quad (20)$$

The comparisons between the predicted and measured peak stress for 30Cr2Ni4MoV steel under different forming temperatures and strain rates are shown in Table 3. Obviously, an agreement between the measured and calculated values is satisfactory.

Determination of the strain corresponding to peak stress

Generally, the peak strain (ε_p) can be considered as,

$$\varepsilon_p = aZ^b, \quad (21)$$

where a and b are both material parameters, while Z is Zener–Hollomon parameter.

Based on the experimental results, the values of Zener–Hollomon parameter can be evaluated from Eq. 20. Then, the values of a and b can be computed as 1.13×10^{-3} and 0.1, respectively, by means of relationship between ε_p and Zener–Hollomon parameter (Fig. 5). So, Eq. 21 can be changed as following,

$$\varepsilon_p = 1.13\times10^{-3}Z^{0.1}. \quad (22)$$

Table 4 shows comparisons between the predicted and measured strain corresponding to peak stress for 30Cr2Ni4MoV steel under test conditions. Obviously, there are large differences between the measured and calculated results.

Therefore, Zener–Hollomon parameter needs to be modified, and the modified Zener–Hollomon parameter (Z^*) can be assumed as,

$$Z^* = \dot{\varepsilon}^k\exp\left(\frac{Q}{RT}\right), \quad (23)$$

where k is the correction coefficient for strain rate. Based on the experimental results and Eq. 20, the value of k can be determined as 2.43. Then, the modified Zener–Hollomon parameter (Z^*) can be described as,

$$Z^* = \dot{\varepsilon}^{2.43}\exp\left(\frac{Q}{RT}\right). \quad (24)$$

Similarly, the values of a and b can be computed as 4.46×10^{-2} and 7.09×10^{-2}, respectively. Therefore, Eq. 21 can be modified as,

$$\varepsilon_p = 4.46\times10^{-2}(Z^*)^{0.07}. \quad (25)$$

Table 5 shows the comparisons between the experimental and predicted results by Eq. 25 for

Table 3 Comparison between predicted and measured peak stress

Temperature (°C)	Strain rate (s^{-1})								
	0.001			0.01			0.1		
	Measured	Predicted	Relative error/%	Measured	Predicted	Relative error/%	Measured	Predicted	Relative error/%
950	60.17	62.34	3.61	89.23	89.34	0.12	128.22	117.75	−8.17
1050	39.99	35.67	−10.80	56.17	58.03	3.31	84.99	84.60	−0.46
1150	21.79	19.92	−8.58	38.33	35.55	−7.25	55.82	57.88	3.69
1250	12.51	11.54	−7.75	21.92	21.51	−1.87	40.27	38.03	−5.56

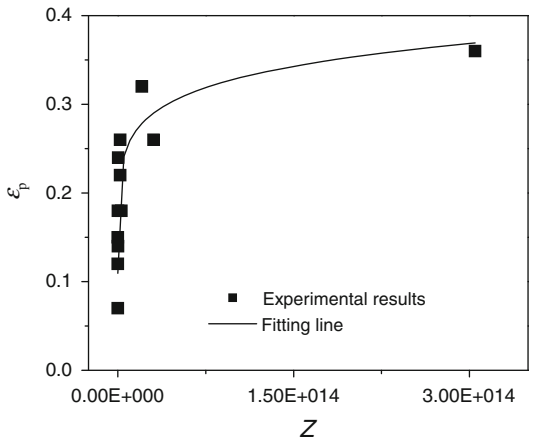

Fig. 5 Relationship between ε_p and Zener–Hollomon parameter

30Cr2Ni4MoV steel under test conditions. Obviously, a good agreement between the measured and calculated values is obtained, and the maximum relative error is only 5.32%.

Verification of the developed constitutive equations

According to the above analysis and discussion, the developed constitutive models for 30Cr2Ni4MoV steel under hot deformation can be summed as,

$$\begin{cases} \sigma = \sigma_p\left[1-\left(\dfrac{\varepsilon_p-\varepsilon}{\varepsilon_p}\right)e^{L\varepsilon}\right] \\ L = -0.8\dot{\varepsilon}^{-0.16}e^{0.002T} \\ \varepsilon_p = 4.46\times10^{-2}(Z^*)^{0.07} \\ Z^* = \dot{\varepsilon}^{2.43}\exp[3.625\times10^5/(RT)] \\ Z = \dot{\varepsilon}\exp[3.625\times10^5/(RT)] \\ \sigma_p = \dfrac{1}{0.022}\ln\left[\left(\dfrac{Z}{3.148\times10^{11}}\right)^{1/3.544} + \sqrt{\left(\dfrac{Z}{3.148\times10^{11}}\right)^{2/3.544}+1}\right]. \end{cases} \quad (26)$$

In order to verify the derived constitutive models, Eq. 26, comparisons between the experimental and predicted results were carried out. Figure 6 show the comparisons between predicted and measured flow stress curves of 30Cr2Ni4MoV steel under four different strain rates and forming temperatures. It can be easily found that the proposed constitutive equations give an accurate and precise estimate of the flow stress for 30Cr2Ni4MoV steel.

Conclusions

In this study, a phenomenological constitutive model has been proposed to describe dynamic deformation behavior

Table 4 Comparisons between the predicted and measured strain corresponding to peak stress

Temperature (°C)	Strain rate (s^{-1})								
	0.001			0.01			0.1		
	Measured	Predicted	Relative error/%	Measured	Predicted	Relative error/%	Measured	Predicted	Relative error/%
950	0.180	0.228	26.67	0.260	0.290	11.54	0.360	0.369	2.50
1050	0.140	0.172	22.86	0.220	0.219	−0.45	0.320	0.279	−12.82
1150	0.120	0.135	12.50	0.180	0.172	−4.44	0.260	0.219	−15.77
1250	0.100	0.109	9.00	0.150	0.139	−7.33	0.240	0.177	−26.25

Table 5 Comparisons between the predicted and measured strain corresponding to peak stress

Temperature (°C)	Strain rate (s^{-1})								
	0.001			0.01			0.1		
	Measured	Predicted	Relative error/%	Measured	Predicted	Relative error/%	Measured	Predicted	Relative error/%
950	0.180	0.170	−5.56	0.260	0.253	−2.69	0.360	0.377	4.72
1050	0.140	0.141	0.71	0.220	0.209	−5.00	0.320	0.311	−2.81
1150	0.120	0.119	−0.83	0.180	0.178	−1.11	0.260	0.264	1.54
1250	0.100	0.104	4.00	0.150	0.154	2.67	0.240	0.229	−4.58

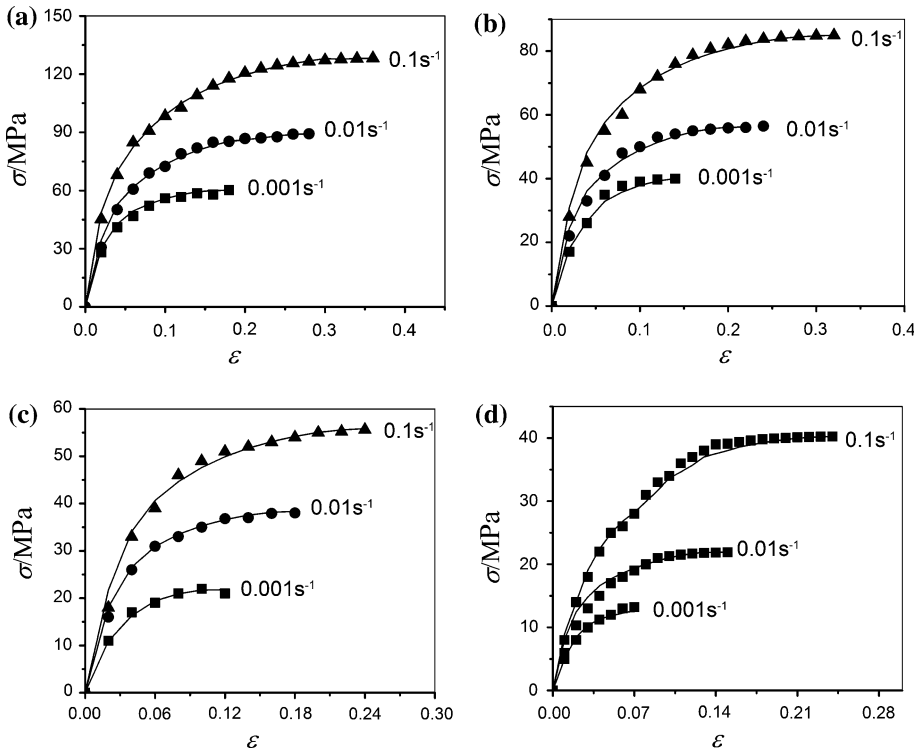

Fig. 6 Comparison between predicted and measured flow stress curves of 30Cr2Ni4MoV steel under four different strain rates and forming temperatures of **a** 950 °C, **b** 1050 °C, **c** 1150 °C, and **d** 1250 °C

of 30Cr2Ni4MoV steel in wide strain rate, strain, and temperature regimes. Among the proposed constitutive model, L parameter is sensitive to the forming temperature and strain rate and indicates the attenuation degree of the flow stress. So, L parameter can be also defined as the attenuation coefficient before the peak stress. Meanwhile, the mathematical equations to predict peak stress and peak strain corresponding to peak stress were established. By the compensation of strain rate, one modified Zener–Hollomon parameter is put forward to improve the prediction accuracy of constitutive model of peak strain. Comparisons between the experimental and predicted results were carried out and confirmed that the proposed deformation constitutive model presented an accurate and precise estimate of the flow stress for 30Cr2Ni4MoV steel and can be used to realize numerical simulation of forging and establish the hot formation processing parameters for 30Cr2Ni4MoV steel.

References

1. Lin YC, Chen XM (2011) Mater Des 32:1733. doi:10.1016/j.matdes.2010.11.048
2. Lin YC, Liu G (2010) Comput Mater Sci 48:54
3. Spathis G (2007) J Mater Sci 42:5815. doi:10.1007/s10853-006-1441-5
4. Plaseied A, Fatemi A (2008) J Mater Sci 43:1191. doi:10.1007/s10853-007-2297-z
5. Lin YC, Chen MS, Zhong J (2008) Comput Mater Sci 42:470
6. Lin YC, Xia YC, Chen XM, Chen MS (2010) Comput Mater Sci 50:227
7. Lin YC, Chen MS, Zhong J (2008) Mech Res Commun 35:142
8. Lin YC, Chen XM, Liu G (2010) Mater Sci Eng A 527:6980
9. Lin YC, Chen XM (2010) Comput Mater Sci 49:628
10. Zerilli FJ, Armstrong RW (2007) J Mater Sci 42:4562. doi:10.1007/s10853-006-0550-5
11. Lin YC, Chen MS (2009) Mater Sci Eng A 501:229
12. Lin YC, Chen MS (2009) J Mater Sci 44:835. doi:10.1007/s10853-008-3120-1
13. Lin YC, Zhong J, Zhong J (2008) Comput Mater Sci 43:752
14. Lin YC, Liu G, Chen MS, Zhong J (2009) J Mater Proc Technol 209:4611
15. Toros S, Ozturk F (2010) Appl Soft Comput. doi:10.1016/j.asoc.2010.06.004
16. Wang YP, Han CJ, Wang C, Li SK (2011) J Mater Sci (under review)
17. Hockauf M, Meyer LW (2010) J Mater Sci 45:4778. doi:10.1007/s10853-010-4595-0
18. Lopes W, Corrêa ECS, Campos HB, Aguilar MTP, Cetlin PR (2009) J Mater Sci 44:441. doi:10.1007/s10853-008-3121-0
19. Zener C, Hollomon H (1944) J Appl Phys 15:22
20. Sellars CM (1966) Acta Met 14:1136
21. Lin YC, Chen MS, Zhong J (2008) J Mater Proc Technol 205:308
22. Ko BC, Yoo YC (2000) J Mater Sci 35:4073. doi:10.1023/A:1004838305228
23. Cho SH, Yoo YC (2001) J Mater Sci 36:4279. doi:10.1023/A:1017995122420
24. Aghaie-Khafri M, Golarzi N (2008) J Mater Sci 43:3717. doi:10.1007/s10853-008-2604-3